

Reduced Impact of Frequency Dithering on the Performance of High-Order Modulation Format Phase Conjugation

A. A. I. Ali^{1,*}, T. T. Nguyen^{1,†}, S. Boscolo¹, S. Takasaka², R. Sugizaki², and A. D. Ellis¹

¹Aston Institute of Photonic Technologies, Aston University, Birmingham, B4 7ET, United Kingdom

²Furukawa Electric Co. Ltd, 6 Yawata-kaigandori, Ichihara, Chiba, 290-8555, Japan

*aliaai@aston.ac.uk. †Now with Infinera PA, 7360 Windsor Dr, Allentown, PA 18106, USA

Abstract: We address the primary degradations in optical phase conjugation devices, reducing the implementation penalty to below 0.2dB and enabling, for the first time, performance improvement in a 400-km long probabilistically shaped 256-QAM transmission system. © 2021 The Author(s)

1. Introduction

Optical phase conjugation (OPC) can be used for extending the transmission reach and (or) increasing the link capacity through the simultaneous compensation of fibre nonlinearity and dispersion [1]. Currently, the nonlinearity compensation benefits of fibre-based OPC are masked by the penalty associated with its insertion. This is variously attributed to signal-to-noise ratio (SNR) degradation (a tradeoff between conversion efficiency (CE) and intra-channel nonlinearity [2]) and phase modulation effects [3]. A dual counter-dithered pump OPC configuration [4] is commonly used to increase the stimulated Brillouin scattering (SBS) threshold resulting in high CE and, at the same time, reduce the transferred phase from the dithered pumps to the conjugate signal (through four-wave mixing). Nevertheless, the dither transfer is not canceled completely but some residual dither is still transferred to the conjugate signal as a result of imperfect matching between the radio-frequency (RF) amplifiers and optical modulators [5]. This dither penalty may be avoided by omitting dither (at the expense of CE) [6], or by the use of SBS-free nonlinear elements such as semiconductor optical amplifiers (at the expense of conversion bandwidth) [7] or nonlinear crystals (at the expense of insertion loss or device complexity).

For quadrature-amplitude modulation (QAM) signals, at present the lowest dithering penalties are restricted to 1 dB and 2 dB for 16- and 64-QAM [8, 9], respectively, and prevent the use of the dithered dual-pump OPC scheme with 256-QAM. In [10], a penalty of 1 dB in the frequency shifting of a 64-QAM signal was achieved by use of counter dithering with a single frequency tone. In this paper, we improve the counter dithering scheme in dual-pump OPC such as to reduce the penalty to 0.2 dB for both shaped and unshaped 256-QAMs. This negligible implementation penalty enables the demonstration of a record mutual-information (MI) increase of 0.5 bits/symbol/polarisation for 256-QAM and 0.4 bits/symbol/polarisation for probabilistically shaped (PS) 256-QAM. In addition, we demonstrate improved resilience to misalignment of the counter dithering in a back-to-back configuration by use of a dithering compensation algorithm in the receiver digital signal processing (DSP) block.

2. Experimental Setup

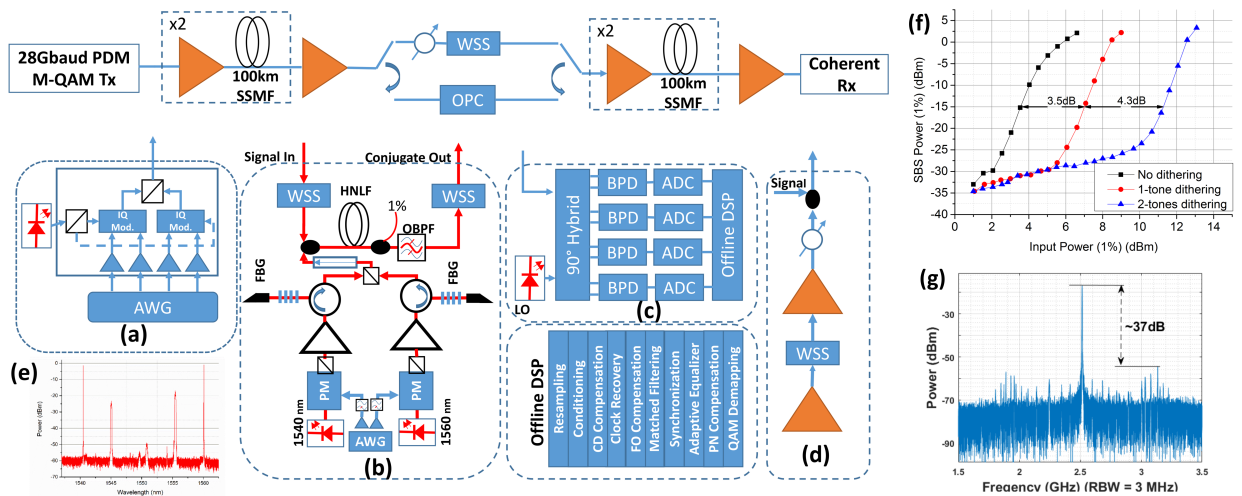


Fig. 1. Experimental setup of the lumped amplification system with mid-link OPC. (a) Transmitter for 28-Gbaud PDM M-QAM signals, (b) dual-pump polarisation-independent OPC, (c) coherent receiver with block diagram of the offline DSP, (d) noise loading setup, (e) OPC spectrum after the HNLF, (f) 1% of SBS power versus 1% of input power to the HNLF, and (g) RF spectrum of the coherently received conjugated CW signal with optimised dithering.

The experimental setup is depicted in Fig. 1, where Fig. 1(a) shows the 28-Gbaud polarisation division multiplexing (PDM) M -QAM transmitter. The symbols of uniform QAM and PS QAM (following the Maxwell-Boltzmann distribution with a shaping factor of 0.09 [11]) were time-multiplexed with 5% quadrature phase-shift keying pilot symbols periodically (1 pilot in every 19 payloads) for use in the data-aided algorithm of the receiver DSP [9]. The data was oversampled (2 samples/symbol) and filtered, then loaded in an arbitrary waveform generator (AWG) with a sampling rate of 56GSa/s. The 4 data channels were sent to 45-Gbaud IQ modulators, and an external cavity laser at wavelength 1555.75 nm was used as a continuous-wave (CW) signal source. Figure 1(b) shows the setup of the dual-pump OPC. Two CW lasers located at 1540.5 nm and 1560.1 nm (line-widths of < 10 kHz and < 100 kHz, respectively) were used as pump sources. Two almost identical sets of two RF tones (60 MHz and 600 MHz) were amplified using RF amplifiers, filtered using 700-MHz low pass filters and used to counter-phase modulate the pumps by external phase modulators, so to increase the SBS threshold of the HNLF. A polarisation controller with a polarisation beam splitter was used to improve the degree of polarisation of the two CW laser signals. The laser signals were then amplified using two high-power erbium-doped fibre amplifiers (EDFAs) and filtered (to suppress amplified spontaneous emission (ASE) noise) using circulators and fibre Bragg gratings (1-nm bandwidth and centred at the pump wavelength). The two pumps were combined using a polarisation beam combiner. The signal was filtered using a wavelength selective switch (WSS) (to increase the CE), and combined with the two orthogonal pumps using a 3-dB coupler, then propagated in a highly nonlinear fibre (HNLF; length = 100 m, zero-dispersion wavelength = 1550 nm, loss $\alpha = 1.2$ dB/km, nonlinear coefficient $\gamma = 21.4$ W/km, and dispersion slope = 0.041 ps/nm²/km at 1550 nm). A tunable optical bandpass filter was used at the output of the HNLF to suppress the pumps. Lastly, a WSS filtered out the signal and residual pump waves at the OPC output. Figure 1(e) shows the optical spectrum at the 1% monitoring coupler located at the output of the HNLF. The spectrum shows around -6 -dB CE, giving an overall insertion loss (ratio of signal input to conjugated output) of -19 dB. The transmission link comprised 4 spans of 100-km standard single-mode fibre ($\alpha = 0.2$ dB/km, dispersion = 17 ps/nm/km, $\gamma = 1.3$ W/km) and an EDFA (6-dB noise figure) at the beginning of each span. In the middle of the link, either the signal passed through the OPC, or its conjugate was propagated in the second half of the link, or the signal bypassed the OPC device. A variable optical attenuator (VOA) with a WSS was used in the path without OPC to ensure that the same input power was injected in the second half of the link in both cases (with and without OPC), hereby producing the same noise accumulation in the second half of the link. Signal detection was performed using a polarisation diverse coherent receiver (Fig. 1(c)), in which the signal (or conjugate) was combined with a local oscillator (< 100 kHz line-width) and set to 1555.75 nm (or 1544.75 nm) in the 90° optical hybrid. Four balanced photodiodes were located at the hybrid output and real-time sampling oscilloscopes (100GSa/s, 33-GHz analogue bandwidth) worked as analogue-to-digital converters. The sampled data was processed offline using a desktop computer [9]. The system performance was evaluated using the SNR and the MI measured directly from the recovered data with the aid of the transmitted payloads [9].

3. Results and Discussion

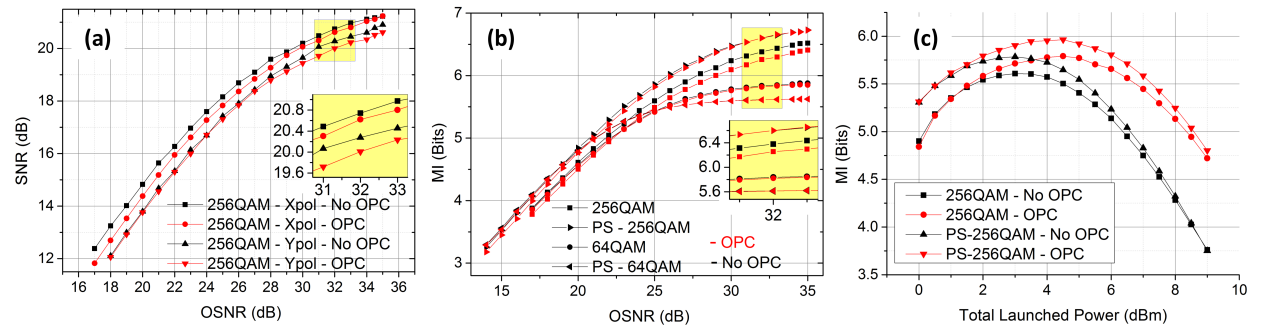


Fig. 2. (a) SNR as a function of the OSNR for the two polarisations of the 256-QAM system in back-to-back setup. (b) MI for different modulation formats as a function of the OSNR. (c) Transmission results for the MI as a function of the total launched power in 4×100 -km span. All the results are shown with and without the OPC.

Figure 1(f) shows the SBS power reflected from the HNLF as a function of the input power. The SBS was measured by connecting the output of the circulator after the high-power EDFA (for the 1540 nm signal) directly to the input of the HNLF, and a 2×2 1% monitoring coupler was used at the input of the HNLF to measure the input and reflected powers. When using a single dithering tone, the SBS threshold was increased by around 3.5 dB, and an additional 4.3 dB was achieved by using two tones. To characterise the residual dithering, a CW laser signal was used as the input signal to the HNLF, and the resulting conjugate was mixed coherently with another CW laser signal (separated by 2.5 GHz) by a 3-dB coupler, and the output was captured with a photodiode connected to a RF spectrum analyser. Figure 1(g) shows the RF spectrum of the received conjugate, which features approximately 37-dB residual dithering suppression compared to the carrier. This improved suppression was achieved by optimising the amplitude of the RF

dithering tones to make the pump phases at the output of the phase modulators identical and setting the counter-phase so that to account for the path difference between the two pumps.

With the optimised dithering, we tested the conjugation of different high-order modulation formats at a 28-Gbaud symbol rate. In these measurements, as shown in Fig. 1(d), ASE noise from an EDFA (shaped with the WSS and swept using a VOA) was combined with the transmitted signal (and conjugated signal in the OPC case), amplified and connected to the receiver. Figure 2(a) shows the measured SNR of the uniform 256-QAM signal as a function of the optical SNR (OSNR). We observe ~ 0.2 -dB penalty due to the OPC insertion for both polarisations. The results for different modulation formats are summarised in Fig. 2(b), and show negligible penalty due to the OPC insertion for the PS 256-QAM and 64-QAM formats. We ascribe the penalty reduction with respect to the uniform 256-QAM case to the increased phase margin of 64-QAM or the reduced occurrence of corner constellation points in PS 256-QAM. Figure 2(c) shows the MI of uniform and PS 256-QAM signals as a function of the total launched power in 4 spans of 100km SSMF (Fig. 1). We can see around 0.5-bit/symbol improvement at the optimum launched power for both formats. The shaping, optimised for an OSNR of 25 dB (3-dBm launched power), clearly improves the performance by a further 0.3 bit/symbol, but this shaping gain gradually decreases in the high-power region where the Gaussian impairment assumption is no longer valid.

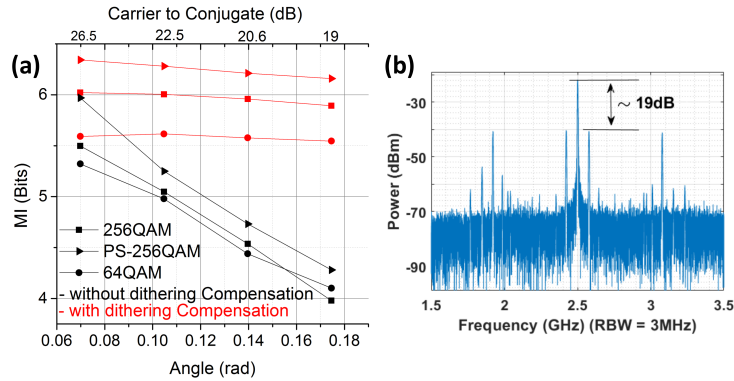


Fig. 3. (a) MI (measured at 36-dB OSNR) as a function of the pump-phase mismatch with and without digital compensation, and (b) RF spectrum of coherently received conjugated CW signal for 0.175-rad pump-phase mismatch.

With less precise pump counter-dithering, the OPC performance gain disappears. To make the system robust to imperfect matching between the two pump phases, we added a data-aided phase-noise compensation algorithm to the DSP block after the conventional phase-noise compensation unit at the receiver, which blindly searched and compensated the deterministic phase distortion induced by the pump dithering [12]. To test the algorithm, we repeated the results shown in Fig. 2(b) at 35-dB OSNR with imperfect dithering. Figure 3(a) shows the MI of different modulation formats (64-QAM, uniform and PS 256-QAMs) as a function of the phase mismatch angle (measured relative to optimum dithering). The results show that the dithering degrades the performance significantly, by around 1.5 bits/symbol, which corresponds to a suppression of the residual dither sidebands by only 19 dB below the carrier. In contrast, even at large pump-phase mismatches, adding the dithering compensation stage removes the majority of these penalties, thereby providing substantial tolerance against imperfect dithering.

4. Conclusion

We have demonstrated the OPC of high-order modulation formats with 0.2-dB SNR penalty for uniform 256-QAM and almost zero penalty for PS 256-QAM and the lower-order formats. Using optimised pump counter-dithering, we have transmitted a 28-Gbaud PDM 256-QAM signal over a 400-km link, and demonstrated a nonlinearity compensation gain of around 0.5 bits/symbol in the MI, giving a predicted data rate of 308 Gbit/s and 317 Gbit/s for uniform and PS 256-QAM, respectively (compared to 298 Gbit/s and 308 Gbit/s without OPC).

Acknowledgments: This work was supported by the UK ESPRC Grants EP/S016171/1, and EP/S003436/1.

References

1. M. A. Z. Al-Khateeb *et al.*, *Opt. Express* **26**, 23960–23968 (2018).
2. I. Sackey *et al.*, *Proc. ECOC*, IEEE, 2014.
3. R. Elschner *et al.*, *IEEE J. Sel. Top. Quantum Electron.* **14**, 666–673 (2008).
4. A. A. I. Ali *et al.*, *Proc. OFC*, OSA, 2019.
5. A. A. I. Ali *et al.*, *Proc. ECOC*, IEEE, 2019.
6. G. Saavedra *et al.*, *Proc. OFC*, OSA, 2018.
7. D. Marcenac *et al.*, *Electron. Lett.* **33**, 879–880 (1997).
8. H. Hu *et al.*, *Proc. OFC*, OSA, 2016.
9. S. Namiki *et al.*, *Proc. OFC*, OSA, 2016.
10. H. N. Tan *et al.*, *Proc. OECC*, IEEE, 2015.
11. T. Nguyen *et al.*, *IEEE J. Lightwave Technol.* **39**, 388–399 (2020).
12. T. T. Nguyen *et al.*, Submitted, 2021.